"Rainbow" trapped in a self-similar coaxial optical waveguide

Qing Hu, Jin-Zhu Zhao, Ru-Wen Peng,[a] Feng Gao, Rui-Li Zhang, and Mu Wang
National Laboratory of Solid State Microstructures and Department of Physics, Nanjing University, Nanjing 210093, China

(Received 6 November 2009; accepted 29 March 2010; published online 19 April 2010)

We report in this paper that the light waves with different frequencies can be selectively guided and spatially separated in a self-similar dielectric waveguide, where a hollow core is surrounded by a coaxial Thue–Morse multilayer. Due to the self-similar furcation feature in the photonic band structure, the transmission multibands are achieved. More interestingly, this dielectric waveguide supports "cladding modes," which are spatially separated and confined along the waveguide. Consequently, a "rainbow" can be trapped (spatial confined but not stopped) in the Thue–Morse waveguide. The finding can be applied to designing miniaturized compact photonic devices, such as spectroscopy on a chip. © *2010 American Institute of Physics*. [doi:10.1063/1.3399778]

Nowadays great efforts have been devoted in manipulating light signals in order to make photons as an alternative carrier for information transfer.[1,2] New principles and technology for trapping, storing, and releasing light signals become extremely important. Various schemes have been proposed to trap the light. For example, by introducing defects in photonic crystals, photons can be localized in the structures[3] Very recently, the spatial separation of optical spectrum and the formation of a trapped "rainbow" in metamaterials have been theoretically demonstrated at both terahertz frequencies and telecommunication wavelengths.[4] In a sense, these artificial structures play the role of "waveguides."

It is well known that waveguides confine and guide the light waves, and play an important role in the modern optoelectronics and telecommunications.[5,6] An optical waveguide is usually made of dielectric materials. Optical waveguides have mainly two obvious disadvantages: polarization dependence and miniaturization limit. Recently, some progresses have been made to solve these problems by wrapping the guiding core with photonic crystals (PCs).[7,8] However, conventional hollow-core designs give the narrow transmission bands, and the baneful dispersive resonances that grow with increasing number of identical subcavities. Very recently, a chirped photonic crystal fiber[9] has been fabricated to localize the reflection of different wavelengths at different layers of the structure, which broadens the narrow transmission bands and suppresses the detrimental dispersive resonance. In this paper, by introducing a self-similar waveguide we present a unique scheme to achieve transmission multibands and overcome detrimental dispersive resonance, further to realize the spatial separation of frequency-selective light waves. This kind of waveguide cannot only guide optical modes like a PC fiber, it can also trap light as a "rainbow" (spatial confinement but not "stopping" of light).

The self-similar dielectric waveguide (SDW) is designed with a hollow core surrounded by coaxial Thue–Morse multilayer. The Thue–Morse sequence is one of the well-known 1D aperiodic structures.[10,11] The Thue–Morse sequence contains two building blocks A and B and can be produced by repeating application of the substitution rules $A \rightarrow AB$ and $B \rightarrow BA$. In the SDW [as schematically shown in Fig. 1(a)], the coaxial Thue–Morse multilayer consists of two building blocks A and B with refraction indexes n_A and n_B, thicknesses d_A and d_B, respectively. In the following calculations, the radius of the hollow core is set as $R_0=3.8a$, the refraction indexes as $n_A=4.6$ and $n_B=1.6$, and their thicknesses as $d_A=0.33a$ and $d_B=0.67a$, respectively. Here a is the characterized size of the SDW, which corresponds to the operating wavelength of the waveguide. For example, the waveguide can operate at optical frequency if $a=100$ nm. Figures 1(b) and 1(c) illustrate the refractive-index distributions in the SDWs with the generations S_6 and S_7, respectively. It is obvious that the refractive indexes distribution is nonperiodic, and it presents self-similarly along radial axis of the SDW. Actually, the self-similarity also exists among neighboring generations, for example, the refractive-index distribution of the generation S_7 is an enlarged analogy of the generation S_6 [as shown in Figs. 1(b) and 1(c)].

By applying the transfer matrix method in cylindrical coordinate system,[12] the photonic band structure of the SDW can be numerically calculated. Figure 2 illustrates the photo-

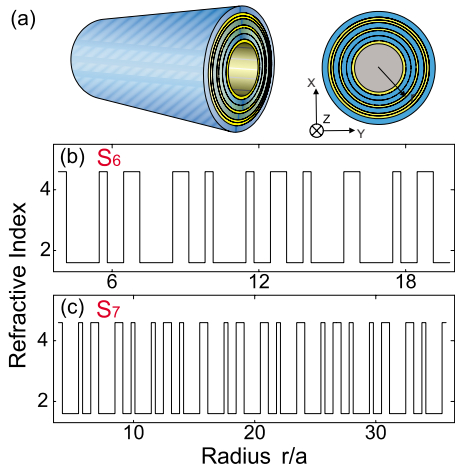

FIG. 1. (Color online) (a) The schematic SDW (left) and its cross section (right). In the SDW, a hollow core (refractive index $n_0=1$) is surrounded by a coaxial Thue–Morse multilayer consisting of two building blocks A (yellow layer) and B (blue layer). The refractive-index distributions in the SDWs with different generations: (b) S_6 and (c) S_7, respectively.

[a]Author to whom correspondence should be addressed. Electronic mail: rwpeng@nju.edu.cn.

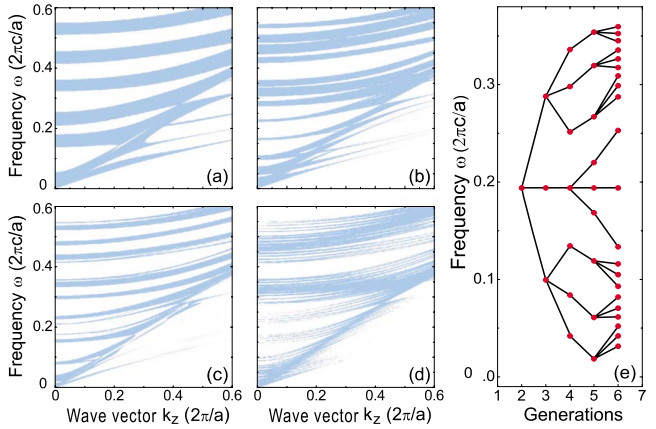

FIG. 2. (Color online) The calculated photonic band structures of the SDW, which contains the cladding Thue–Morse dielectric multilayer with different generations S_n: (a) S_3; (b) S_4; (c) S_5; and (d) S_6, respectively. Note that the PBGs are for both TE and TM polarizations. (e) The central frequency distribution of the PBGs in the SDW with different Thue–Morse generations.

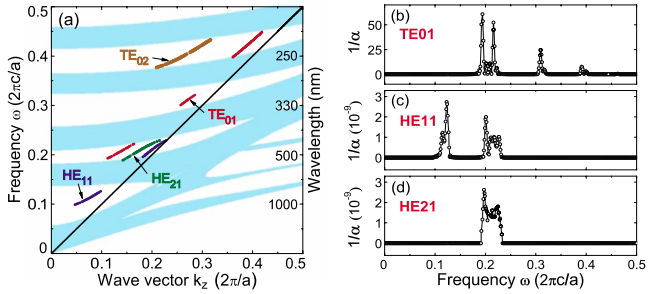

FIG. 3. (Color online) (a) The transmission modes in SDW with the generation S_3. The modes are plotted in circles: the red is for TE_{01}, the brown is for TE_{02}, the blue is for HE_{11}, and the green is for HE_{21}. The black solid line is for incident light. (b) The reciprocal of the attenuation $(1/\alpha)$ as a function of frequency for the modes: TE_{01} (top), HE_{11} (middle), and HE_{21} (down), respectively. Here the characterized size of the SDW is $a=100$ nm, thereafter, the SDW works at optical frequency.

nic band structures of the SDW, which contains the cladding Thue–Morse dielectric multilayer with different generations S_n. As shown in Fig. 2, there exists several frequency regions (shown in blue), where the incident plane waves transmit throughout the cladding layers and yet cannot be confined in the SDW; while there also exists the frequency regions (shown in white) where the electromagnetic waves are confined in the SDW, known as the photonic band gaps (PBGs). Note that these PBGs are for both transverse electric (TE) and transverse magnetic (TM) polarizations. Comparing with the periodic dielectric waveguide reported in Ref. 7, in the SDW there are more PBGs at the same frequency range. For example, in the frequency range of $\omega/\omega_0=0-0.5$, two PBGs exist in periodic waveguide (Ref. 7), yet in SDW with S_3 totally five PBGs can be identified [as shown in Fig. 2(a)]. Such a difference originates from the self-similarity in SDW. Furthermore, by increasing the generations of Thue–Morse structure, more PBGs occur at the same frequency region [as shown in Figs. 2(b)–2(d)]. Actually, due to the self-similarity in the structure, the PBGs in the SDW are furcated. Figure 2(e) shows the central frequency of the PBGs in the SDW with different Thue–Morse generations. It follows that each PBG in one generation grows one or three branches for next generation. Therefore, the PBGs in the SDW indeed possess the furcation feature, which create more possibilities in selecting the propagating modes in the waveguide.

The propagating modes in the SDW can be obtained by following the method in Ref. 13. It is shown that in the SDW with S_3, there are the following low-frequency modes [as shown in Fig. 3(a)]: (i) TE_{01} and TE_{02} modes, which belong to transverse electric modes (TE_{ml}). The electric-field of the TE_{ml} modes is purely perpendicular to wave vector. Therefore, it has only three nonzero components of field: E_θ, H_z, and H_r. (ii) HE_{11} and HE_{21} modes, which belong to the TE-like hybrid modes (HE_{ml}). The HE_{ml} modes are hybrid modes which have totally six nonvanishing field components: $E_z, E_\theta, E_r, H_z, H_\theta, H_r$. These propagating modes present interesting features. On one hand, the same type of propagating modes is separated by the PBGs in the SDW. For example, TE_{01} modes exist in three different frequency ranges as $\omega/\omega_0=0.19-0.22$, 0.30–0.32, and 0.39–0.47, respectively. Here $\omega_0=2\pi c/a$. These three frequency ranges do no overlap, implying that the propagating modes are frequency-selective. On the other hand, for different types of propagating modes, the frequency ranges of some modes overlap, and some of them are separated. For instance, in the frequency range of $\omega/\omega_0=0.19-0.23$, TE_{01}, HE_{11}, and HE_{21} modes simultaneously exist. However, in the frequency range of $\omega/\omega_0=0.1-0.15$, only HE_{11} mode exists; and in the range of $\omega/\omega_0=0.25-0.35$, only TE_{01} mode exists. Therefore, the SDW can be used as a multimode waveguide in some frequency ranges, and it can be also used as a single-mode waveguide in other frequency ranges. This feature opens a way to achieve frequency-selective transmission multibands in waveguides.

In order to quantify the transmission performance of the waveguide, we study the attenuation of light wave in the SDW. The attenuation of light wave (α) in the waveguide is defined as the ratio of the radially-outgoing power of the mode to its forward-propagating power in the waveguide as[13]

$$\alpha(\omega) = S_r|_{r=R} \times (2\pi Rl) \Big/ \int_0^l ldz \int_0^{2\pi} d\phi \int_0^R S_z(r,\phi) r dr, \tag{1}$$

where S_r, S_z, are the radial and axial energy flux densities, respectively; R is the outermost radius of the waveguide. For three different modes TE_{01}, HE_{11}, and HE_{21}, we have calculated their attenuation in the SDW as a function of frequency [as shown in Figs. 3(b)–3(d)]. It is obvious that TE_{01}, HE_{11}, and HE_{21} modes propagate in the SDW at some frequency regions, which exactly corresponds to the transmission modes in Fig. 3(a). Besides, TE_{01} mode has much better performance of transmission than HE_{11} and HE_{21} modes. Please note that because the attenuation (α) given in Eq. (1) is a relative ratio, large attenuation of HE_{11} and HE_{21} modes does not mean these modes can not be guided inside the waveguide. Actually, the electromagnetic fields of the HE_{11} and HE_{21} modes are comparable with that of the TE_{01} mode (shown in Fig. 4), and strong enough to be guided in the waveguide.

It should be mentioned that the electromagnetic fields for different modes are spatially separated in different cladding layers of the SDW. The time-average electric-field energy density in the frequency range $(\omega_1-\omega_2)$ can be summed as

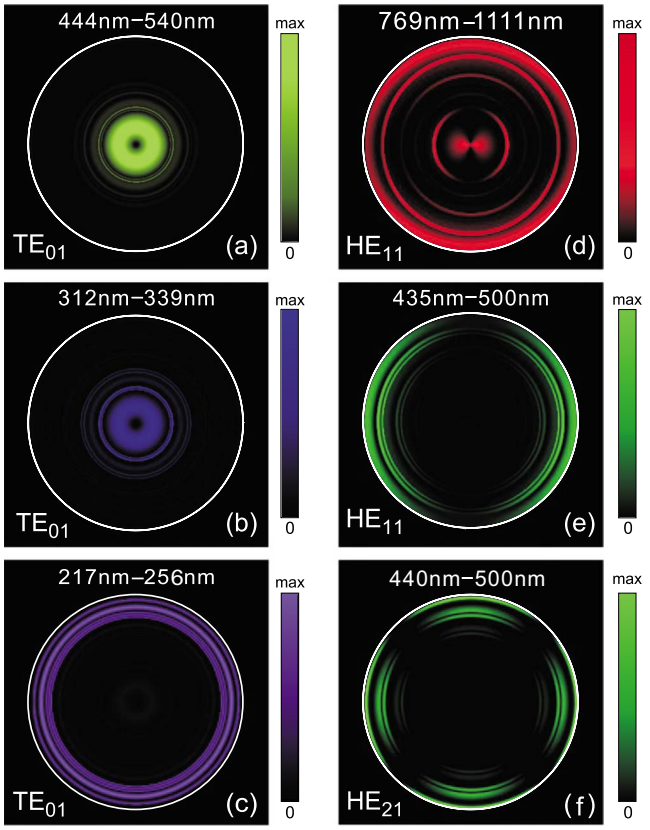

FIG. 4. (Color online) The electric-field time-average energy density distributions in the SDW with the generation S_3 for different modes: (a)–(c) TE_{01} modes, (d)–(e) HE_{11} modes, and (f) HE_{21} modes, respectively. Here the characterized size of the SDW is $a=100$ nm.

$$\Gamma = \frac{1}{2}\int_{\omega_1}^{\omega_2} \varepsilon_r(|\vec{E}(\omega)|)^2 d\omega, \tag{2}$$

where ω_1 and ω_2 are the minimum and maximum frequencies in the range, respectively, and ε_r is the dielectric constant. Based on Eq. (2), we have calculated the electric-field energy density distributions for different modes in the SDW with S_3 (as shown in Fig. 4). It is found that the electromagnetic fields for different modes are spatially separated in different cladding layers. For $a=100$ nm, in TE_{01} mode, the light with the wavelength $\lambda=444-540$ nm is trapped in the core layer [Fig. 4(a)]; the light with $\lambda=312-339$ nm is trapped in both the core layer and the first several cladding layers [Fig. 4(b)]; and the light with $\lambda=217-256$ nm is trapped near the outmost cladding layer [Fig. 4(c)]. For HE_{11} mode, the light with $\lambda=769-1111$ nm is trapped in both the core and the last several cladding layers [Fig. 4(d)]. In fact, the contribution of the electric-field in the core layer is devoted mostly by E_z and E_r, and the electric-field density in the last several cladding layers is, however, devoted mostly by E_ϕ. The light in the band 435–500 nm is trapped near the outmost layers [Fig. 4(e)], mostly devoted by E_z and E_r. For HE_{21} mode, the light in the band 440–500 nm is also trapped near the outmost layer [Fig. 4(f)]. However, the electric-field patterns of HE_{11} mode are different from that of HE_{21} mode because the angular momentum is $m=1$ for HE_{11} mode but $m=2$ for HE_{21} mode.

Therefore, electromagnetic fields with different frequencies are spatially separated in different cladding layers, indicating that a rainbow is formed and can be trapped in the SDW. The physical origin of this feature is the self-similarity in the SDW, which allows the furcation of PBGs and generates more PBGs by increasing the hierarchy of Thue–Morse sequence. Meanwhile, several feature sizes distribute inhomogenously in the Thue–Morse structure, which makes light wave resonates at several different frequencies and the signals with different resonant frequencies propagate in different cladding layers. In this way, the rainbow appears in the SDW. Similar phenomena can be observed in other frequency regions by simply changing the characterized size (a) in the SDW. The finding can be applied to designing miniaturized compact photonic devices, such as a spectroscopy on a chip, color-sorters on a chip, and photon sorters for spectral imaging.[14]

This work was supported by grants from the National Natural Science Foundation of China (Grant Nos. 10625417, 50972057, and 10904061), the State Key Program for Basic Research from the Ministry of Science and Technology of China (Grant Nos. 2010CB630705 and 2006CB921804), and partly by Jiangsu Province (Grant No. BK2008012).

[1] J. S. Foresi, P. R. Villeneuve, J. Ferrera, E. R. Thoen, G. Steinmeyer, S. Fan, J. D. Joannopoulos, L. C. Kimerling, H. I. Smith, and E. P. Ippen, Nature (London) **390**, 143 (1997).
[2] J. Zi, J. Wan, and C. Zhang, Appl. Phys. Lett. **73**, 2084 (1998).
[3] S. Noda, A. Chutinan, and M. Imada, Nature (London) **407**, 608 (2000).
[4] K. L. Tsakmakidis, A. D. Boardman, and O. Hess, Nature (London) **450**, 397 (2007); Q. Gan, Y. J. Ding, and F. J. Bartoli, Phys. Rev. Lett. **102**, 056801 (2009).
[5] S. E. Miller and A. G. Chynoweth, *Optical Fiber Telecommunications* (Academic, New York, 1979).
[6] B. E. A. Saleh and M. C. Teich, *Fundamentals of Photonics* (Wiley, New York, 1991).
[7] M. Ibanescu, Y. Fink, S. Fan, E. L. Thomas, and J. D. Joannopoulos, Science **289**, 415 (2000); M. Ibanescu, S. G. Johnson, M. Soljacic, J. D. Joannopoulos, and Y. Fink, Phys. Rev. E **67**, 046608 (2003).
[8] B. Temelkuran, S. D. Hart, G. Benoit, J. D. Joannopoulos, and Y. Fink, Nature (London) **420**, 650 (2002).
[9] J. S. Skibina, R. Iliew, J. Bethge, M. Bock, D. Fischer, V. I. Beloglasov, R. Wedell, and G. Steinmeyer, Nat. Photonics **2**, 679 (2008).
[10] R. Riklund and M. Severin, J. Phys. C **21**, 3217 (1988); C. Godreche and J. M. Luck, J. Phys. A **23**, 3769 (1990); M. G. Qin, H. R. Ma, and C. H. Tsai, J. Phys.: Condens. Matter **2**, 1059 (1990).
[11] F. Qiu, R. W. Peng, X. Q. Huang, X. F. Hu, M. Wang, A. Hu, S. S. Jiang, and D. Feng, Europhys. Lett. **68**, 658 (2004); N. H. Liu, Phys. Rev. B **55**, 3543 (1997).
[12] Y. Xu, G. X. Ouyang, R. K. Lee, and A. Yariv, J. Lightwave Technol. **20**, 428 (2002).
[13] S. G. Johnson, M. Ibanescu, M. Skorobogatiy, O. Weisberg, T. D. Engeness, M. Soljacic, S. A. Jacobs, J. D. Jonannopoulos, and Y. Fink, Opt. Express **9**, 748 (2001).
[14] E. Laux, C. Genet, T. Skauli, and T. W. Ebbesen, Nat. Photonics **2**, 161 (2008).